Assignments 2: Kinematic Analysis

For this second assignment we studied all the three mechanisms proposed by the paper shared and already considered for the first assignment. The report is divided into three main chapters and a concluding part. The first chapter describes the 2D kinematic model of the different mechanism, the second contains the kinematic analysis, while the third contains considerations about kinematic engineering specifications and performance indices. In each chapter there is a section specifically dedicated to each of the three mechanisms in which considerations, images, graphs and results are given

Before moving on to the actual study, we consider it appropriate to state here a few considerations that apply to all three mechanisms.

Mechanism size

As mentioned in the first assignment, the DRS mechanism must respect certain constraints imposed by the FIA. Previously, we did not bother to mention these constraints imposed by the regulations for the sake of brevity. However, since in this second assignment we had to actually design the mechanism in 2D, it was essential to stick to these constraints and we feel it necessary to mention the most important ones here. The regulations we followed are those of the championships of the years 2021[1] and 2022[2], the official links are given in the notes.
Briefly, the side view of everything related to the rear wings of the vehicle (i.e. main wing, flap wing, pylon and drs) must be enclosed in a **box whose length does not exceed 350mm and whose height does not exceed 220mm**.
Another constraint specified by the regulation would be that the distance between the two section of the Rear Wing Profile (i.e. the main wing and the flap wing) must lie between 10mm and 15mm at their closed position and between 10mm and 85mm when the DRS system is deployed (chapter 3.6.3 of 2021 regulation[1] and 3.10.10 of 2022 regulation[2]). In our studies we followed what the professor suggested and we fixed these two distances to be: **10mm when the mechanism is closed and 50mm when the DRS is open**.

Wing choice

While looking for information about DRS, we found a paper containing an aerodynamic study of six possible configurations for the rear wings of a Formula One car. You can find it at the link reported in the notes[3].
Together with other information that will certainly be useful in the dynamic study of mechanisms, at the end of the paper there is a table (Table 10) containing the results of the various configurations. The conclusion is that the configuration with the highest L/D ratio (lift over drag ratio) adopts the short BE50 airfoil as the shape for the main wing and the NACA 2415 airfoil for the flap wing. The chord lengths adopted by the paper and that we also decided to use (in compliance with the FIA regulations) are **290mm for the main wing and 120mm for the flap wing**.
In addition to the measurements, we also used these wing shapes in the drawing of the three mechanisms to make them more real.

Plotting references

For plotting, we used, in addition to the plottools library and Maple's standard display command, the visualisation package MBSymbaRenderer from Professor F. Biral.

---

[1] https://www.fia.com/sites/default/files/2021_formula_1_technical_regulations_-_iss_10_-_2021-06-28.pdf
[2] https://www.fia.com/sites/default/files/formula_1_-_technical_regulations_-_2022_-_iss_11_-_2022-04-29.pdf
[3] https://iopscience.iop.org/article/10.1088/1757-899X/243/1/012030

2D kinematic model of the solutions

In our project we analyse the three possible mechanisms for the actuation of the DRS.
From a kinematic description point of view, the *push-up* type was described using the global formulation, while the *pod-pull* and the *pod-rocker* via the recursive approach. All the mechanisms possess only one degree of freedom. In all the models we used *s* (the axial displacement of the slider of the piston) as the independent variable, since our goal is to correlate the opening of the wing with the moving of the piston.
All aspects concerning the absolute position of the arms (global case) or the angles relative to the local reference frame (recursive case) were synthesised through dependent variables.
For each mechanism we defined a reference frame in the body for the global formulation and in the joint for the recursive formulation, respectively.
An auxiliary reference frame for the flap wing was defined, in order to plot it rotating dynamically together with the opening of the mechanism. The link connecting the piston mechanism to the wing is not attached to the leading edge of the flap wing but in the middle, so that we can achieve a configuration where we reach the maximum opening of the wing allowed by the regulations. Finding the right set of parameters of the system (lengths of the link, position of the points fixed to the ground) was challenging, because we often incurred in changes of configurations during the position analysis, despite the fact that we derived analytical solutions.

1. Push-up type

The *push-up* mechanism exploited the early design of the F1 cars, which relied on a pylon to support the rear wing. The hydraulic actuator is placed inside the pylon, pushing the flap from the bottom.
The system was described using the global formulation. The number of links is equal to three, connected via one prismatic joint and two revolute joints: in this way we obtain a system of 9 equations in 9 dependent variables. From the project reference paper (Dimastrogiovanni), the link connecting the piston to the wing has a more complex geometry, but in the kinematic analysis it is sufficient to model it using a straight link connecting the joints.

2. Pod-pull type

The *pod-pull* mechanism reduces the size of the pod. The hydraulic actuator directly pulls the link to the flap in order to open the wing.
The system was described using the recursive formulation: the number of links is equal to three, connected via one prismatic joint and two revolute joints. There is only one kinematic loop, so we obtain two constraint equations in two dependant variables, the relative angles ψ_1 and ψ_2 of the revolute joints.

3. Pod-Rocker type

In the *pod-rocke*r mechanism, the hydraulic actuator is placed in a pod mounted above the rear wing's top surface, and then it pulls on a rocker in order to increment the leverage of the piston. The rocker is then connected to the edge of the flap wing by a link. A mechanism like this is not enough to guarantee the desired movement of the piston: an extra degree of freedom is required. Many solutions can be implemented, like allowing an horizontal movement of the lower vertix of the rocker via a cam joint. We decided to adopt a revolute joint on the left edge of the piston, so that the rotation of the rocker is not constrained by the prismatic joint of the piston.
The first kinematic model we implemented used a global approach: since the number of links of the mechanism is equal to 6, the overall number of variables was 19 (we use the extra variable *s*), with a system of 18 constraint equations. Solving this system requires a very high computational effort and we never get a solution, so we decided to switch to the recursive formulation. This approach is easier to compute and therefore Maple is able to provide us with an analytical solution. The constraint equations are obtained by connecting the two possible kinematic loops, so the number of equations is equal to four, since it is a 2D description.
Fixing *s* as the independent variable, the dependant variables are the ψ_1, ψ_2, ψ_5, ψ_6. which express the relative rotations in each revolute joint. The geometric angles described by the rocker are computed using the law of cosines, using the lengths of the links as input data.

Despite the low number of equations, we still had to substitute all the parameters of the system before solving the constraint equations, otherwise the analytical solution would have gotten too complicated.

Kinematic analysis

The kinematic analysis performed on the three mechanisms is divided into three sub-studies: position analysis, inverse kinematics and velocity analysis.
We know from the theory that the **position analysis** includes both the **initial configuration problem** and the **finite displacement analysis**. We summarised the results of both the studies for all the three mechanisms in a drawing that changes depending on the value of the independent variable *s*. From the initial configuration problem we generally got many solutions for the constraint equations, and we kept the one which resembles our mechanism. The dynamic drawing is done with the *animate* function that calls the *draw_mechanism* procedure with different values of *s*: because we have an analytical solution it is not necessary to implement an actual finite displacement analysis.
In order to understand how much we have to move the piston to guarantee a specified distance between the main wing and the flap we had to compute the **inverse kinematic**. Given the complexity of the kinematic relation, we adopted the non-linear optimizer *NLPSolve* from the *Optimization* library of Maple. The cost function we pass to this optimizer consists in the difference between the wings distance obtained through the kinematic solution (expressed in terms of *s*) and the desired wings distance. The result of the optimization is a value of *s* that tells how much the piston has to be moved in order to zero the cost function. As described in the last chapter, we particularly used the inverse kinematic to compute the stroke the piston has to travel to open the wing from the closed configuration. The results we got are very precise, the order of magnitude of the error is of 10^{-20}.
To finish the position analysis, in addition to the wings, the pylon, the arms, the revolute joints and the piston of the mechanism, we also drew with dashed lines the **working space** of each of the different moving parts.
Regarding the **velocity analysis**, we do not have much to add to what we have seen in theory. For each of the mechanisms we calculated the **velocity ratio** between the variable representing the flap wing angle and the independent variable s. We did not find it necessary to calculate the same ratio for other dependent variables.

1. Push-up type

a) Position analysis

Solving the constraint equations we obtained two different solutions for the initial position problem.

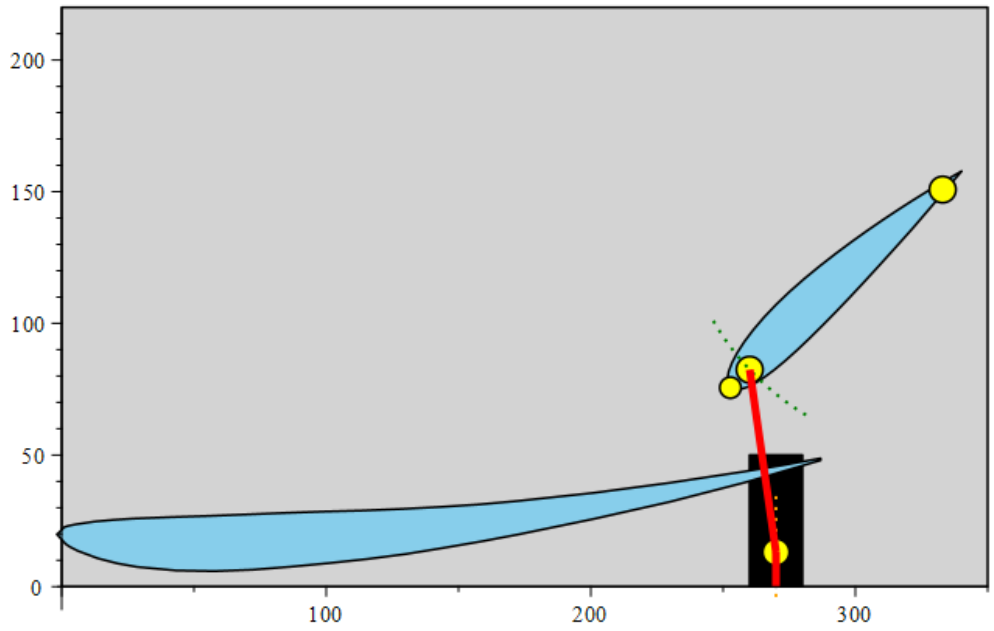

b) Velocity analysis

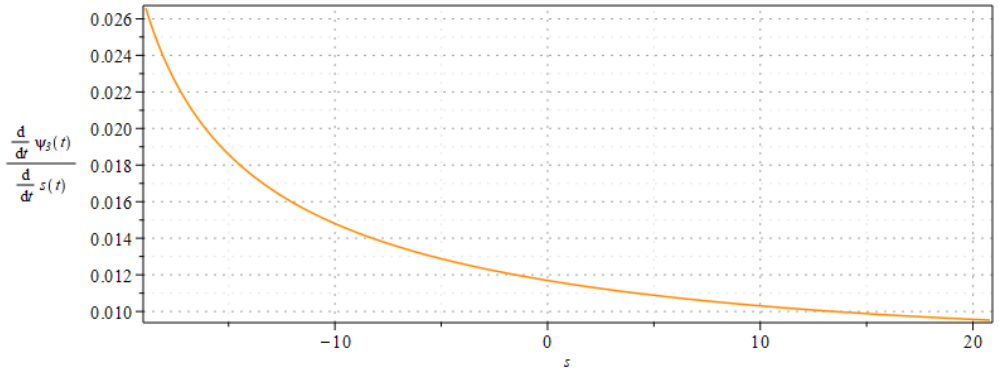

In figure the velocity ratio for the flap wing angle is represented. In all the configurations the velocity ratios will be displayed in the interval of *s* that was found in the inverse kinematics section: the values of the displacement *s* that are in between the initial and final configurations. Comparing this plot to the ones of the other mechanisms, it is clear how the *push-up* system is intrinsically slower than the other two, since the velocity of the flap wing goes down quite fast while the piston pushes forward.

2. Pod Pull type

a) Position analysis

Solving the constraint equations we obtained two different solutions for the initial position problem.

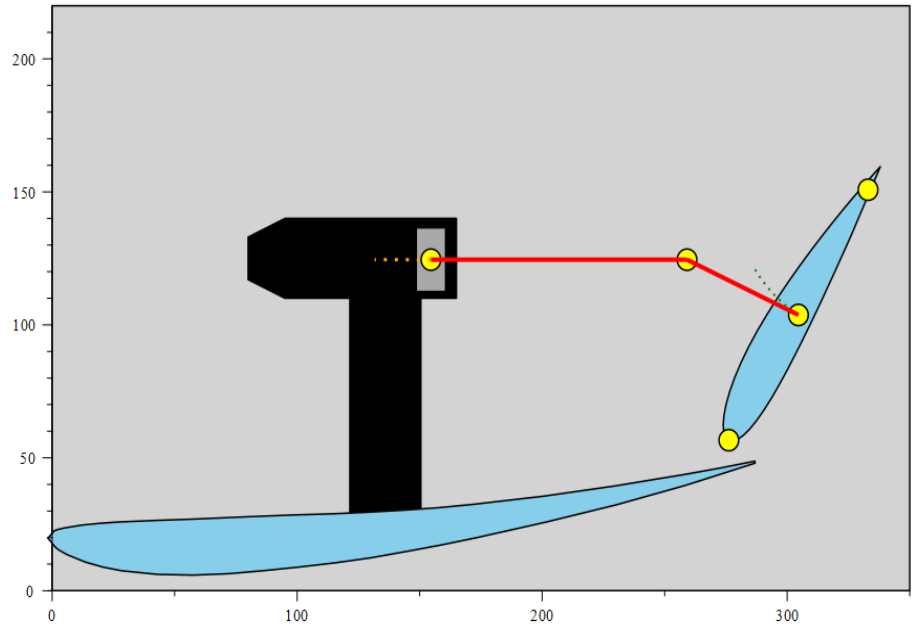

b) Velocity analysis

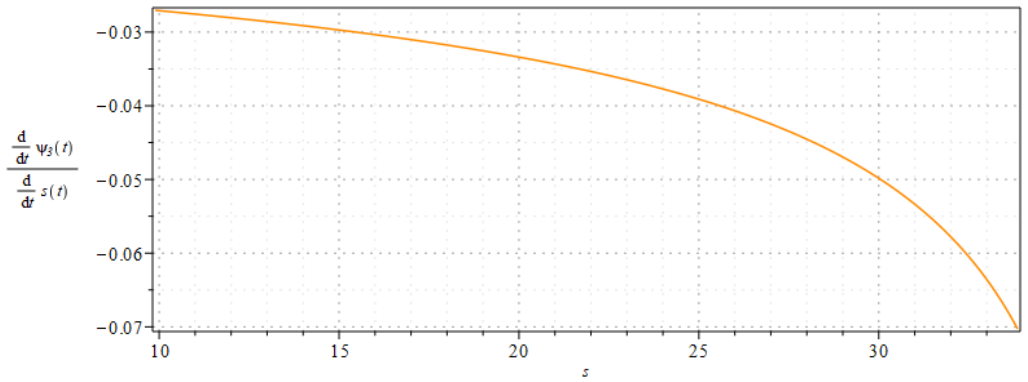

In figure the velocity ratio for the flap wing angle is represented. The velocity ratio is greater than the one of the *pod-pull* mechanism in all the operating interval: this means that this configuration is able to produce greater angular velocities for the flap wing for the same velocity of the piston. This analysis is

purely kinematic and does not take into account the dynamics of the system, but it can still provide a good estimate of the most performing solution in terms of the opening time.

3. Pods & Rocker type

a) Position analysis

Solving the constraint equations we obtained four different solutions for the initial position problem, two of them being complex numbers.

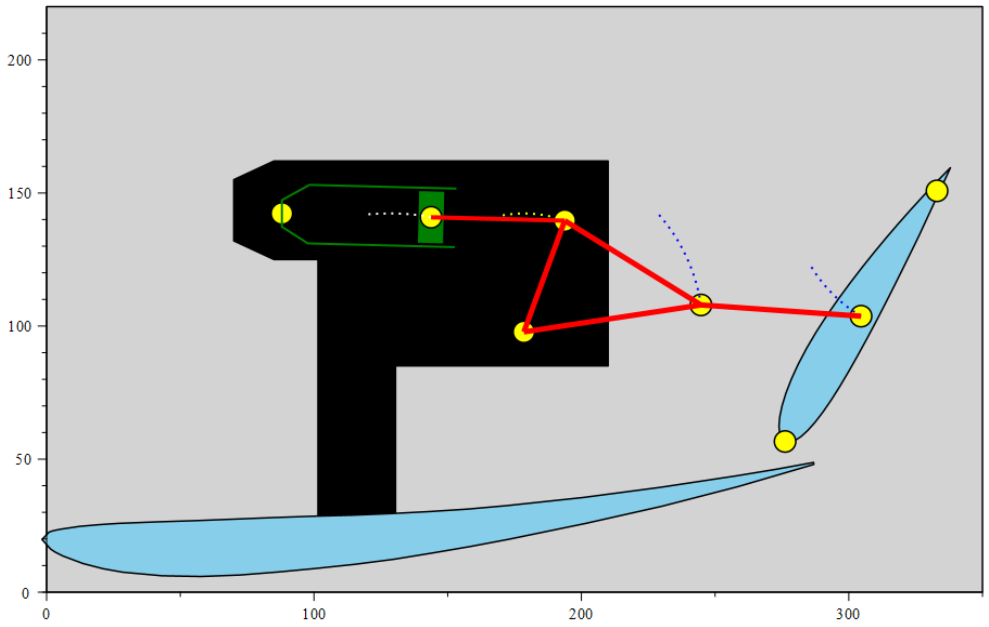

b) Velocity analysis

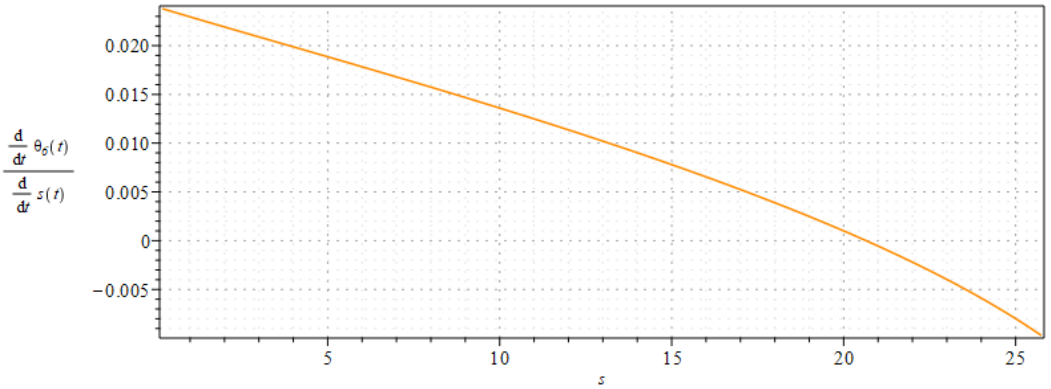

In figure the velocity ratio for the flap wing angle is represented.

Kinematic engineering specifications and performance indices

In this first assignment, concerning the kinematic analysis of the mechanisms, there are not many relevant performance indices, since the dynamics really plays a crucial role in studying the system. For instance, many indices are related to vibrations, work, power, forces and stresses, which require a dynamic analysis.

A performance analysis that has been already carried out in this report is the one concerning the velocity ratios between the angular velocity of the flap wing and the velocity of the slider of the piston. The main goal of the optimization of the mechanism is to minimise the opening time of the flap wing, so a greater velocity ratio describes the potential of the system to reach higher velocities, only from a kinematic point of view.

For each mechanism we also measured the piston stroke that is necessary in order to get from the *closed* configuration to the *opened* one. Generally speaking, in this first stage of the simulation, we can assume that the longer the stroke, the slower the opening of the mechanism will be. The required stroke was computed as

the difference between the values taken by the variable *s* in the opened and closed configurations.

To give these values a better visualisation we computed the opening time of all the mechanisms by defining an actuation law for the piston which is the standard one for robotics: the motion is uniformly accelerated in the first half of the opening time and decelerated in the second half, by guaranteeing a zero final velocity for the piston. We were not able to find any information about the real actuation laws actually used by the piston, but since this is a very general analysis our time law can be considered as acceptable. In fact, using this motion is suitable for minimising the residual vibrations.
The results are summarised in the table at the end of the chapter.

Piston stroke & Opening time
2 crucial kinematic specifications are piston stroke and opening time.
The first one is determined through inverse kinematics: minimising 2 costs function initial and final piston position are identified. Results are reported in the table below and show how pod pull, with the current configurations in slight advantage with a smaller variation. *Push-up*, due to a different connection with the moving wing is characterised by a much larger stroke.
Given the piston stroke we were able to calculate the opening time of each mechanism by imposing the motion profile of the piston. We chose a base profile that minimises the residual vibration caused by the otherwise abrought stop of the piston at the end of the stroke. The base profile is reported below. As expected, a shorter piston stroke corresponds to a lower time interval, although all fall in the neighbourhood of 0.1 seconds.

$$baseprofile = \begin{cases} q_{in} + a_{max}\frac{t^2}{2}, & \text{if } 0 \leq t \leq T/2 \\ q_{in} + a_{max}\frac{T^2}{4} - (T-t)^2\frac{a_{max}}{2}, & \text{if } T/2 < t \leq T \end{cases}$$

	Pod-rocker type	**Pod-pull type**	**Push-up type**
Piston stroke [mm]	**25,55**	**23.9706**	**39.6930**
Opening time [s]	**0.1011**	**0.09792**	**0.1260**

Conclusion
Looking at the data reported above it seems like *pod-pull* has a slight advantage over the others, but we are aware that variations in the lengths of the bars and, in general, of the configurations, may change this statement. *Pod-rocker*, given its complicated structure, offers more freedom in the configuration settings and therefore could perform better.
This will be further tested during the dynamic analysis and the optimization process.